JPE 16-3-21

http://dx.doi.org/10.6113/JPE.2016.16.3.1036
ISSN(Print): 1598-2092 / ISSN(Online): 2093-4718

An Active Output Filter with a Novel Control Strategy for Passive Output Filter Reduction

Kyusik Choi† and Bo-Hyung Cho*

†,*Department of Electrical and Computer Engineering, Seoul National University, Seoul, Korea

Abstract

This paper presents a novel control strategy for passive output filter reduction using an active output filter. The proposed method achieves the dual-function of regulating the output voltage ripple and output voltage variation during load transients. The novel control strategy allows traditional simple voltage controllers to be used, without requiring the expensive current sensors and complex controllers used in conventional approaches. The proposed method is verified with results from a 125-W forward converter.

Key words: Passive output filter reduction, Voltage ripple, Load transient, Efficiency

NOMENCLATURE

A_P	Area product.
C_A	AOF capacitor [F].
C_O	Output capacitor [F].
C_P	Post regulator input capacitor [F].
d_A	Duty ratio of AOF.
$\hat{d}_A$	Small signal value of d_A.
D_A	DC value of d_A.
ΔD_{A_OFF}	Ideal D_A variation for forward SW-OFF.
ΔD_{A_ON}	Ideal D_A variation for forward SW-ON.
d_F	Duty ratio of forward converter.
$\hat{d}_F$	Small signal value of d_F.
D_F	DC value of d_F.
f_C	Bandwidth of feedback controller [Hz].
f_{CA}	Bandwidth of AOF controller [Hz].
f_{CF}	Bandwidth of forward converter controller [Hz].
f_{CP}	Bandwidth of post regulator controller [Hz].
f_{Crt}	Critical bandwidth [Hz].
F_{sA}	Switching frequency of AOF [Hz].
F_{sF}	Switching frequency of forward converter [Hz].
F_{sP}	Switching frequency of post regulator [Hz].
i_A	Current from AOF [A].
$\hat{i}_A$	Small signal value of i_A [A].
$<i_A>$	Average i_A during switching period, T_{sA} [A].
i_{CO}	Current into C_O [A].
i_{CA}	Current into C_A [A].
i_{LF}	Current of L_F [A].
I_{LF_pkpk}	Peak to peak value of switching ripple of i_{LF} [A].
i_O	Output current [A].
$\hat{i}_O$	Small signal value of i_O [A].
I_O	DC value of i_O [A].
$I_{O\_\max}$	Maximum I_O [A].
ΔI_O	I_O variation during a load transient [A].
i_{OF}	Output current of separate model [A].
$\hat{i}_{OF}$	Small signal value of i_{OF} [A].
K_{CO_sw}	Output capacitor ratio for switching voltage ripple regulation.
K_{FF_DA}	AOF duty feedforward gain.
K_{AP}	Area product constant.
L_A	AOF inductor [H].
L_F	Forward converter inductor [H].
L_P	Post regulator inductor [H].
n	Transformer turn ratio.
P_{Eft}	Effective power handled by AOF [W].
T_{sA}	Switching period of AOF [s].
T_{sF}	Switching period of forward converter [s].
T_{vA}	Closed loop gain of v_A [s].
T_{vO}	Closed loop gain of v_O [s].
v_A	AOF capacitor voltage [V].
$\hat{v}_A$	Small signal value of v_A [V].
V_A	DC value of v_A [V].
V_{IN}	DC value of input voltage [V].
v_O	Output voltage [V].
$\hat{v}_O$	Small signal value of v_O [V].

Manuscript received Oct. 19, 2015; accepted Dec. 7, 2015
Recommended for publication by Associate Editor Honnyong Cha.
†Corresponding Author: ez2top84@snu.ac.kr
Tel: +82-2-880-1785, Fax: +82-2-878-1452, Seoul National University
*Dept. of Electrical and Computer Eng., Seoul Nat'l University, Korea

ΔV_{O_sw} Output voltage switching ripple [V].
$\Delta V_{O\_sw\_max}$ Output voltage regulation of switching ripple [V].
$\Delta V_{O\_Tr\_max}$ Output voltage regulation of load transient [V].

I. INTRODUCTION

As power semiconductor technology matures, passive output filters (POF), such as LC-filters, accounts for a more significant part of the cost and volume of power converters. Therefore, reducing the POF is one of the most important issues in the design of power converters. However, this reduction is becoming increasingly difficult due to the demanding requirements of digital devices in terms of voltage regulations and efficiency [1]-[3]. Typically, voltage regulations are constraints on the output voltage ripple and on the output voltage fluctuations during load transients [1], [2]. High-frequency switching satisfies both of these regulations. However, the switching frequency is practically upper-bounded due to a proportionally increasing power loss. Thus, a number of studies have been conducted to reduce the POF without high-frequency switching.

For voltage ripple regulation, a passive ripple filter (PRF), an active ripple filter (ARF), and an active output filter (AOF) have been introduced [4]-[13]. The PRF and the ARF show good performance with regard to reducing ripples. However, these methods are overly sensitive to parameter errors [4]-[7], are ineffective owing to their dissipative schemes [8]-[10], or require complex and expensive components [11]-[13]. In addition, they are not suitable for the voltage fluctuation regulation. For voltage fluctuation regulation during a load transient, enhanced-control methods and auxiliary converter methods are typical. Enhanced control methods, such as the V^2 control method [14]-[16], the sliding mode control method [17]-[18], and the linear-and-nonlinear control method [19]-[21], improve the load transient responses under identical hardware conditions. Nevertheless, the enhanced control methods have a limitation given the slew-rates of their output-inductor-currents. To overcome this slew-rate limitation, auxiliary converter methods have been suggested [22]-[25]. Several approaches change the slew-rate using a coupled-inductor for the output-inductor [22]-[23], while the AOF methods inject transient current directly into the output [24]-[25]. These methods are efficient because auxiliary converters handle only a small amount of power. As a result, the auxiliary converters can operate with high-frequency switching and small passive components. However, there are many problems with these devices, such as an expensive coupled inductor [22]-[23] and costly complex controller and current sensors [24], [25]. In addition, these approaches are only for voltage fluctuation regulation. In brief, existing studies provide a single-function for one of the two voltage regulations. Unfortunately, single function methods are generally not sufficient for POF reduction. Although post regulators [26]-[28] have a dual-function for both regulations, they show poor efficiency levels given their series structure.

The conventional AOFs [11], [24], [25] fundamentally share the same structure, indicating that this structure is able to operate for both functions. However, conventional studies have failed to achieve the dual-function because they do not include a proper voltage control strategy or a stability analysis. Moreover, previous studies were not optimized for their own single-functions in spite of their costly current sensors and the complex control methods concealed in their digital controllers.

In this paper, a novel control strategy is proposed for a dual-function AOF. The AOF has the potential for a wide bandwidth control loop given its high-frequency switching. To utilize this property, the main output voltage is controlled by the AOF rather than the main converter. As a result, the output voltage is tightly regulated naturally and a reduced output capacitor is sufficient for load transients. The main converter, on the other hand, controls the voltage of the AOF capacitor. Because there is no given regulation of the voltage, a wider voltage range is available and a small capacitor is sufficient. In addition, the output inductor of the main converter can be reduced because the inductance of the main output inductor is free from the switching voltage ripple due to the proposed method. The switching ripple current from the main converter is cancelled by the AOF and is absorbed into the AOF capacitor. To enhance the switching ripple current cancellation without a current control scheme, a duty feedforward control scheme is also proposed. Finally, it is demonstrated that the proposed dual-function AOF achieves a truly reduced POF.

In Section II, the operation principle of the proposed control strategy is introduced. A small signal analysis and the controller design characteristics are described in Section III. In Section IV, the passive filter reduction process is analyzed and compared to the conventional methods, after which a design guideline for the AOF is described. Section V shows hardware verification results obtained through a 125-W forward converter prototype. Finally, some conclusions are given in Section VI.

II. OPERATION PRINCIPLE

Fig. 1 shows the structure of the proposed system. The main converter is a forward converter and the AOF is a synchronous buck converter. This structure offers two benefits. First, because v_A is not supplied externally, its voltage level is optimized for an efficient AOF [25]. Second, the switching voltage ripple is minimized because the current entering the output capacitor is continuous. In Fig. 2, the control strategies of the conventional AOFs and the proposed AOF are briefly described. The advantages and disadvantages are indicated in green and red, respectively. The conventional AOF for voltage ripple regulation [11]-[13] senses ripple current from the main converter and tracks the sensed current using a hysteresis controller, as shown in Fig. 2(a). The operation of the conventional AOF as a load transient assister [24], [25] is

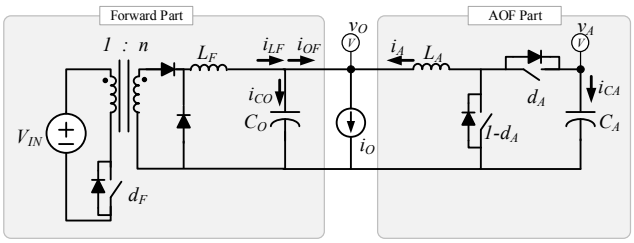

Fig. 1. Structure of the proposed system.

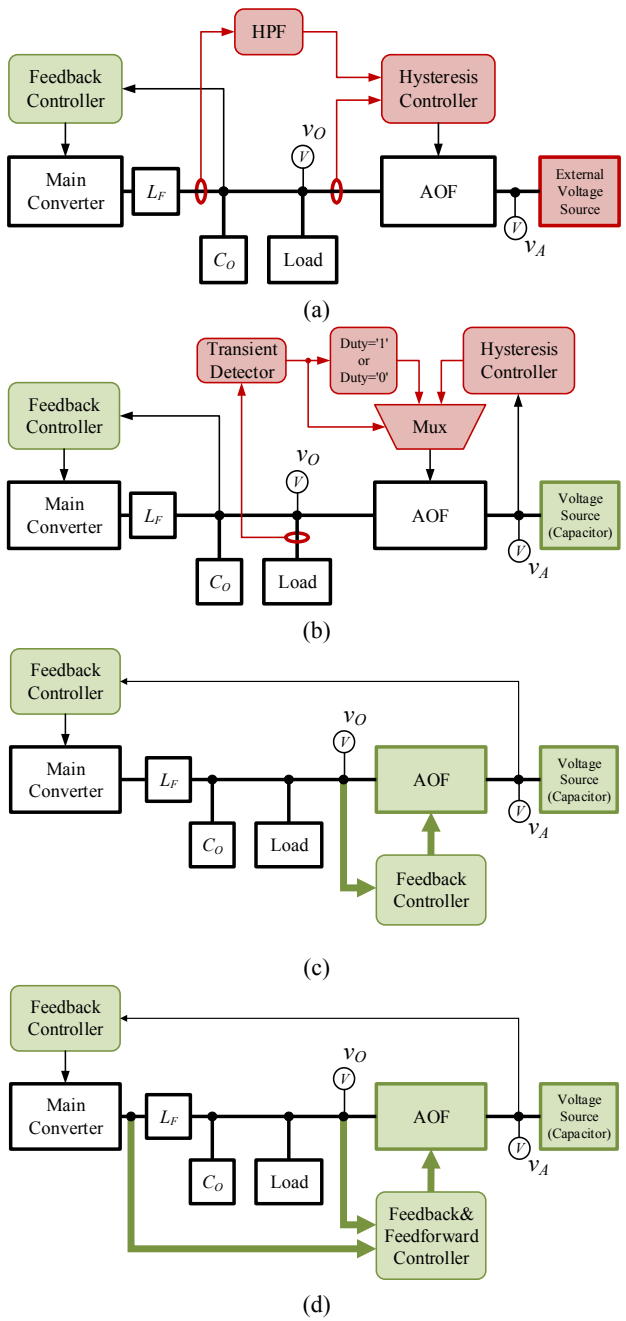

Fig. 2. AOF control strategy and its advantages (green) and disadvantages (red) of, (a) the conventional AOF ripple filter, (b) the conventional AOF load transient assister, (c) the proposed method (w/o feedforward), (d) the proposed method (w/ feedforward).

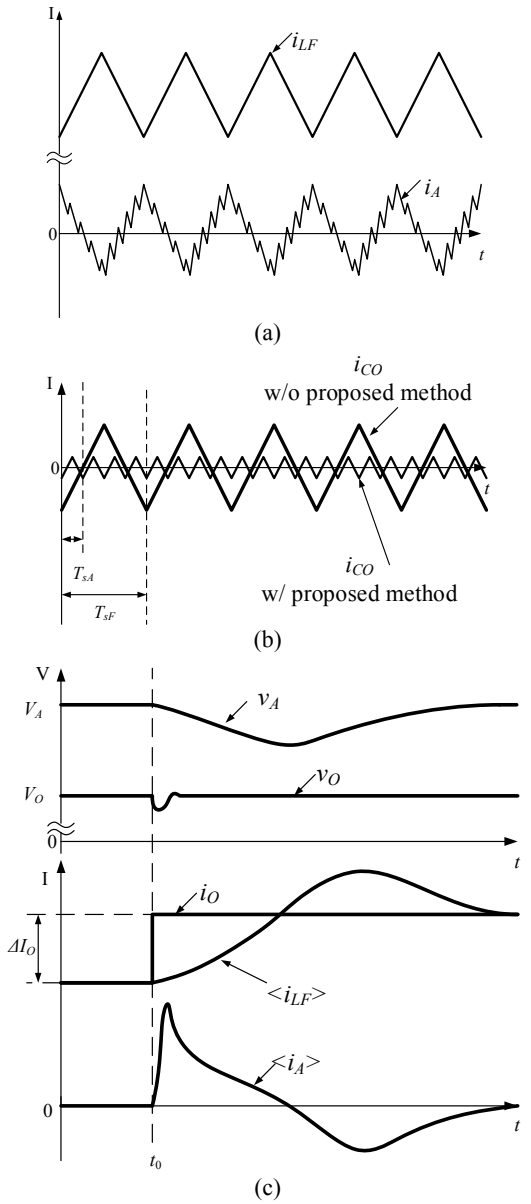

Fig. 3. Key waveforms of, (a) inductor-currents under steady states, (b) currents into the output capacitor w/ and w/o the proposed method, (c) the output voltage, the AOF capacitor voltage, and the average inductor-currents during a step-up (ΔI_O) load transient at t_0.

described in Fig. 2(b). Under steady state conditions, v_A is controlled by the hysteresis controller. In addition, during a load transient, the duty ratio is shown to be fully on/off by the load transient detector. With the proposed method, unlike conventional studies, the output voltage is controlled by the AOF while the voltage of the AOF capacitor is controlled by the main converter, as described in Fig. 2(c). Moreover, the proposed duty feedforward control scheme is utilized to effectively cancel the ripple current without the need for current sensors (see Fig. 2(d)). Detailed descriptions of these processes are given in Section IV.

Fig. 3 shows the key waveforms of the proposed method.

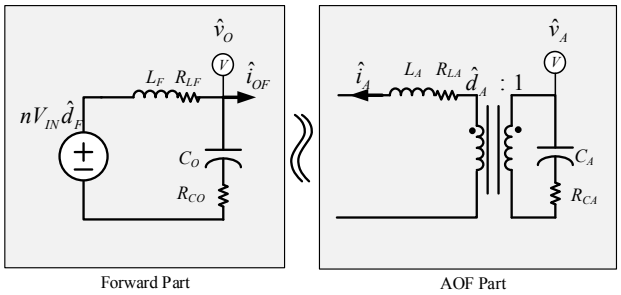

Fig. 4. Separate unterminated model for small signal analysis.

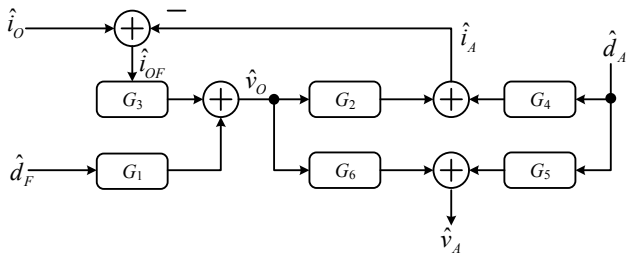

Fig. 5. Structure of the opened-loop small signal model.

TABLE I
TRANSFER FUNCTIONS OF THE SEPARATE UNTERMINATED MODEL

$$G_1 \equiv \left.\frac{\hat{v}_O}{\hat{d}_F}\right|_{seperate} = n\frac{V_{IN}(1+s/w_{ZCO})}{den_F}$$

$$G_2 \equiv \left.\frac{\hat{i}_A}{\hat{v}_O}\right|_{seperate} = \frac{-1}{D_A{}^2}\frac{sC_A}{den_A}$$

$$G_3 \equiv \left.\frac{\hat{v}_O}{\hat{i}_{OF}}\right|_{seperate} = \frac{-R_{LF}\left(1+\frac{s}{w_{ZLF}}\right)\left(1+\frac{s}{w_{ZCO}}\right)}{den_F}$$

$$G_4 \equiv \left.\frac{\hat{i}_A}{\hat{d}_A}\right|_{seperate} = \frac{1}{D_A{}^2}\frac{sC_AV_A}{den_A}$$

$$G_5 \equiv \left.\frac{\hat{v}_A}{\hat{d}_A}\right|_{seperate} = -\frac{V_A}{D_A}\frac{\left(1+\frac{s}{w_{ZCA}}\right)}{den_A}$$

$$G_6 \equiv \left.\frac{\hat{v}_A}{\hat{v}_O}\right|_{seperate} = \frac{1}{D_A}\frac{\left(1+\frac{s}{w_{ZCA}}\right)}{den_A}$$

$$w_{ZCO} = \frac{1}{R_{CO}C_O}$$

$$w_{ZCA} = \frac{1}{R_{CA}C_A}$$

$$w_{ZLO} = R_{LF}/L_F$$

$$den_F = 1+\frac{s}{Q_Fw_{OF}}+\frac{s^2}{w_{OF}{}^2}$$

$$den_A = 1+\frac{s}{Q_Aw_{OA}}+\frac{s^2}{w_{OA}{}^2}$$

$$w_{OF} = 1/\sqrt{L_FC_O}$$

$$Q_F = \frac{1}{R_{LF}+R_{CO}}\sqrt{\frac{L_F}{C_O}}$$

$$w_{OA} = D_A/\sqrt{L_AC_A}$$

$$Q_A = \frac{D_A}{R_{LA}+D_AR_{CA}}\sqrt{\frac{L_A}{C_A}}$$

Under steady state conditions, i_A is controlled, and becomes a counter current of the switching ripple current from the forward converter, as shown in Fig. 3(a). As a result, i_{CO} follows the small switching ripple current of the AOF, as indicated in Fig. 3(b). Thus, a reduced C_O satisfies the requirement of $\Delta V_{O\_sw\_max}$. In addition, L_F can be reduced because I_{LF_pkpk} does not affect i_{CO}. During a load transient event, the dynamic response is greatly improved because the output voltage is controlled by the AOF, which has a wide bandwidth controller according to its high switching frequency

TABLE II
TRANSFER FUNCTIONS OF THE COMBINED SYSTEM

$$G_{vOdF} \equiv \left.\frac{\hat{v}_O}{\hat{d}_F}\right|_{total} = \frac{G_1}{1+G_2G_3}$$

$$G_{vAdF} \equiv \left.\frac{\hat{v}_A}{\hat{d}_F}\right|_{total} = \frac{G_1G_6}{1+G_2G_3}$$

$$G_{vOdA} \equiv \left.\frac{\hat{v}_O}{\hat{d}_A}\right|_{total} = \frac{-G_3G_4}{1+G_2G_3}$$

$$G_{vAdA} \equiv \left.\frac{\hat{v}_A}{\hat{d}_A}\right|_{total} = \frac{G_5(1+G_2G_3)-G_3G_4G_6}{1+G_2G_3}$$

[29]. Fig. 3(c) shows the key waveforms during a step-up (ΔI_O) load transient at t_0. The output voltage, v_O, is tightly regulated, while the AOF voltage, v_A follows the slower dynamic response of the forward converter. As a result, the minimum C_O for load transients is also reduced. Finally, the minimum C_O for both voltage regulations is reduced. Although there are additional passive components, C_A and L_A, a small capacitor is sufficient for C_A due to the absence of tight voltage requirements on v_A. Moreover, the fast switching of the AOF enables a small L_A.

III. SMALL SIGNAL ANALYSIS OF THE AOF

A. Small Signal Model

A small signal model of the AOF is derived in this section to guarantee the stability of the proposed method. An analysis is initially conducted of a separate unterminated model, as shown in Fig. 4, after which the results are combined for the sake of convenience, as shown in Fig. 5. The main parameters, including the equivalent series resistors (ESRs) are shown in Fig. 4. The transfer functions of the separated parts are arranged in Table I. Using the results of the partial analysis, a total small signal model of the power system is derived and shown in Table II.

B. Controller Design

The corresponding closed loop gains of the proposed method are derived as follows:

$$T_1 \equiv H_{vO}G_{vOdA}, \tag{1}$$

$$T_2 \equiv H_{vA}G_{vAdF}, \tag{2}$$

$$T_{vO} \equiv \frac{\hat{y}}{\hat{x}} = T_1 - \frac{H_{vO}H_{vA}G_{vAdA}G_{vOdF}}{1+T_2}, \tag{3}$$

$$T_{vA} \equiv \frac{\hat{w}}{\hat{z}} = T_2 - \frac{H_{vO}H_{vA}G_{vAdA}G_{vOdF}}{1+T_1}. \tag{4}$$

The closed-loop small signal diagrams are shown in Fig. 6. H_{vO} and H_{vA} are the voltage feedback controllers for v_O and v_A, and they determine the bandwidths of T_{vO} and T_{vA}, respectively. Unlike the conventional cases, the proposed control strategy

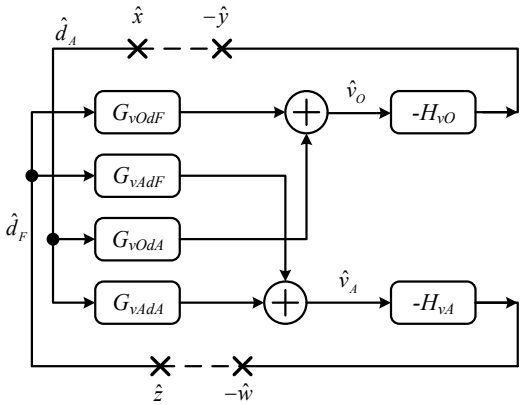

Fig. 6. Diagram of the transfer function of the closed-loop-system with the proposed control strategy.

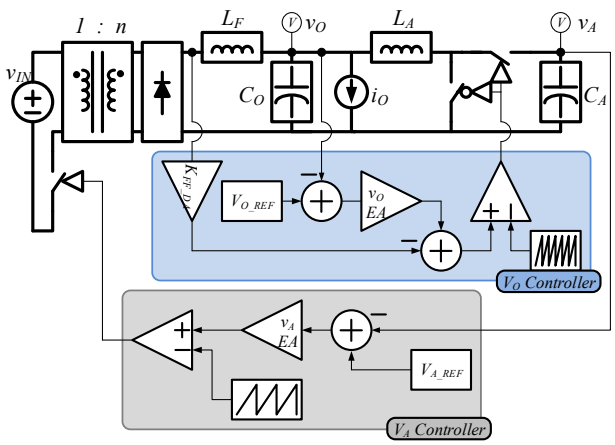

Fig. 7. Proposed system including the duty feed forward.

shows unusual phenomena in the design of the controllers. T_1 shows a zero DC gain owing to the zero DC gain of G_{vOdA}. This phenomenon occurs due to the presence of a non-external voltage source. Fortunately, it disappears after the v_A control loop is closed. Therefore, only the high-frequency gain is considered in the v_O controller design. Finally, T_{vO} has an infinite DC gain and a wide bandwidth. During the H_{vA} design, T_2 shows two unnatural resonant-points. Due to these resonances, there is no phase margin of T_2. However, these resonant points are removed by the other parts of T_{vA} in Equ. (4). This procedure will be shown in detail in Section IV.

C. Duty Feedforward

A traditional voltage feedback controller may not achieve switching ripple current cancellation due to the finite bandwidth of the feedback control loop. Thus, a duty feedforward control method is proposed. The proposed duty feedforward control achieves simultaneous ripple current cancellation with only one additional voltage sensing instance at the rectified point, as shown in Fig. 7. To cancel the ripple current of i_{LF}, the slew rate of $<i_A>$ should be matched to the slew rate of i_{LF}, as follows.

$$\frac{di_{LF}}{dt} = -\frac{d<i_A>}{dt}, \tag{5}$$

where $<i_A>$ refers to the average i_A during a switching period, T_{sA}. The slew rate of i_{LF} is shown below.

$$\frac{di_{LF}}{dt} = \begin{cases} \dfrac{V_{IN}n - V_O}{L_F} & (Forward\ SW-ON) \\ -\dfrac{V_O}{L_F} & (Forward\ SW-OFF). \end{cases} \tag{6}$$

The variation of d_A to satisfy Equ. (5) during the forward-switch-on and switch-off times is derived as follows:

$$\frac{V_{IN}n - V_O}{L_F} = \frac{V_O - (D_A + \Delta D_{A\_ON})V_A}{L_A}, \tag{7}$$

$$\frac{-V_O}{L_F} = \frac{V_O - (D_A + \Delta D_{A\_OFF})V_A}{L_A}, \tag{8}$$

$$\Delta D_{A\_OFF} - \Delta D_{A\_ON} = K_{FF\_DA} V_{IN} n, \tag{9}$$

$$\text{where} \quad K_{FF\_DA} \equiv \frac{L_A}{V_A L_F}. \tag{10}$$

As a result, $-i_A$ is matched to the switching ripple current from the forward converter. This method is even valid when there are certain errors in the parameters, such as the transformer turn ratio, the input voltage, and the leakage inductor. In addition, the proposed feedforward scheme rarely affects the H_{vO} design because the feedforward scheme enhances the average model in the small signal analysis of the forward converter, as presented in Section III. *A*. Although the feedforward affects v_A, the voltage variation is attenuated as the gain of T_{vA} at F_{sF}. Finally, the proposed feedforward scheme does not affect the stability of the system.

IV. Converter Design

As mentioned earlier, an AOF with high-frequency switching is possible because the power loss of an AOF is insignificant due to its low effective power as follow:

$$P_{Eft} \equiv V_O \langle |i_A| \rangle, \tag{11}$$

$$\text{where} \quad \langle |i_A| \rangle \cong \frac{1}{T_{sF}} \int_0^{T_{sF}} |i_{LF} - i_O| dt = \frac{1}{4} I_{L_{LF}\_pkpk}. \tag{12}$$

As a result, the power loss of the AOF is determined by I_{LF_pkpk} rather than by I_O. For example, P_{Eft} is only 5% of the rated power, under the condition of I_{LF_pkpk}=0.2I_{O_max}.

A. Capacitor Reduction

The output voltage is determined by i_{CO}, as follows:

$$v_O = V_O + \int \frac{i_{CO}}{C_O} dt + R_{CO} i_{CO}. \tag{13}$$

Through the cancellation of the switching ripple current, the switching voltage ripple is determined by the AOF as:

$$\Delta V_{O\_sw} = \frac{1}{L_A C_O} \frac{V_A D_A (1-D_A)}{8 F_{sA}^{\ 2}} + R_{CO} \frac{V_O (1-D_A)}{L_A F_{sA}}, \tag{14}$$

and the result should satisfy $\Delta V_{O\_sw} \leq \Delta V_{O\_sw\_max}$. From Equ. (14), the minimum output capacitance of the switching voltage

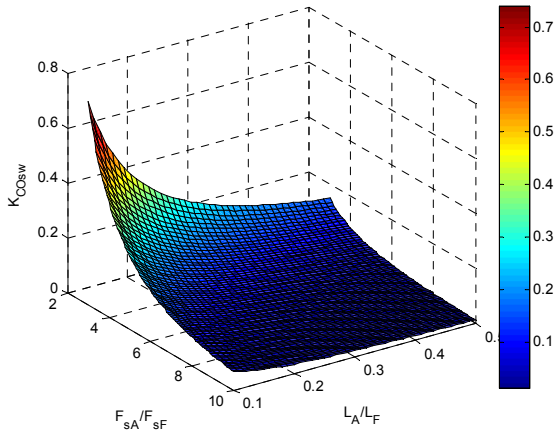

Fig. 8. Minimum output capacitance ratio.

ripple regulation, $C_{O\_sw\_\min}$ is determined as follows:

$$C_{O\_sw\_\min} = \frac{1}{\Delta V_{O\_sw\_\max} - \frac{R_{CO}V_O(1-D_A)}{L_A F_{sA}}} \frac{V_A D_A (1-D_A)}{8 L_A F_{sA}^2}. \quad (15)$$

If the ESR of the output capacitor, R_{CO} is negligible, a comparison of the minimum output capacitances of the proposed system, $C_{O\_sw\_AOF\_\min}$ and the conventional system, $C_{O\_sw\_SF\_\min}$ proceeds as follows.

$$C_{O\_sw\_AOF\_\min} = K_{CO\_sw} C_{O\_sw\_SF\_\min}, \quad (16)$$

$$\text{where} \quad K_{CO\_sw} = \frac{L_F}{L_A} \frac{F_{sF}^2}{F_{sA}^2} \frac{V_A D_A (1-D_A)}{V_{IN} n D_F (1-D_F)}. \quad (17)$$

Fig. 8 shows an example of K_{CO_sw} versus the inductance ratio, L_A/L_F, and the frequency ratio, F_{sA}/F_{sF}, under the D_A=0.5 and D_F=0.25 conditions. K_{CO_sw} decreases dramatically when F_{sA}/F_{sF} increases even when L_A/L_F is 0.2.

According to [29], the peak output voltage variation during a load transient is derived as follows.

$$\Delta V_{O\_Tr\_\max} \begin{cases} \cong \frac{1}{8}\frac{1}{C_O f_C}\Delta I_O & when \quad f_C < f_{Crt} \\ = R_{CO}\Delta I_O & when \quad f_C \geq f_{Ctr}, \end{cases} \quad (18)$$

where f_C is the bandwidth of the feedback controller and f_{Crt} is the critical bandwidth, which is determined as follows.

$$f_{Crt} = \frac{1}{4 R_{CO} C_O}. \quad (19)$$

Thus, the minimum output capacitance, $C_{\_Tr\_AOF\_\min}$ for a load transient when $f_C < f_{Crt}$ is:

$$C_{O\_Tr\_AOF\_\min} = \frac{1}{8}\frac{1}{\Delta V_{O\_Tr\_\max} f_{CA}} |\Delta I_O|, \quad (20)$$

As is well known, the bandwidth of a feedback controller is proportional ($1/10^{th}$ approximately) to the switching frequency. Therefore, the bandwidth of the proposed method is higher by as much as F_{sA}/F_{sF} when compared to the forward converter, and $C_{O\_Tr\_AOF\_\min}$ is reduced.

Finally, the minimum output capacitance is determined with the following criterion:

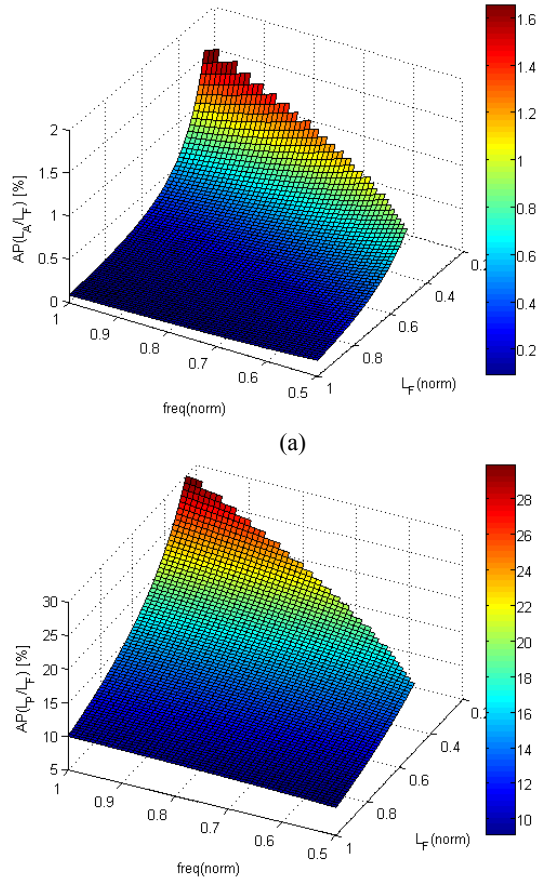

Fig. 9. A_P-ratio of additional inductors compared to L_F of, (a) the proposed method, (b) the post regulator method.

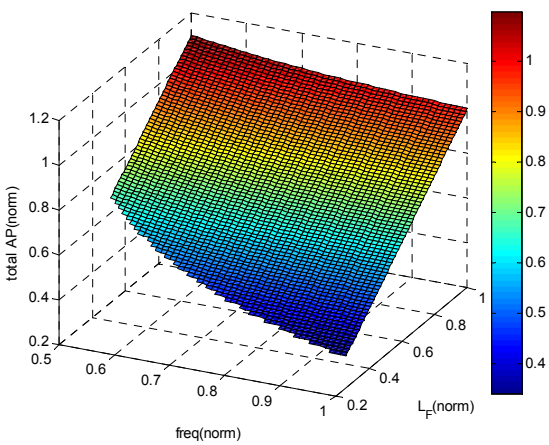

Fig 10. Total A_P of the proposed method.

$$C_{O\_AOF} \geq \max\left(C_{O\_Tr\_AOF\_\min}, C_{O\_sw\_AOF\_\min}\right). \quad (21)$$

The minimum AOF capacitance of the load transients, $C_{A\_Tr\_\min}$ is designed using the same equations for the C_O design, Eqs. (13)-(21), while the maximum variation is set to ±20% rather than ±5%, as follows.

$$C_{A\_Tr\_\min} = \frac{1}{8}\frac{1}{\Delta V_{A\_Tr\_\max} f_{CF}} \Delta I_O D_A, \quad (22)$$

TABLE III
PASSIVE COMPONENT INFORMATION

L_F (AOF)	22 μH (PQ3535)
L_F (SF)	50 μH (PQ4040)
L_F (PR)	22 μH (PQ3535)
L_A	4.7 μH (PQ2020)
L_P	4.7 μH (PQ3230)
C_O (AOF)	47 μF (Ceramic capacitor) 4.7 mF (Electrolytic capacitor)
C_O (SF)	300 μF (Ceramic capacitor) 14.1mF (Electrolytic capacitor)
C_O (PR)	47 μF (Ceramic capacitor) 4.7 mF (Electrolytic capacitor)
C_A, C_P	10 μF (Ceramic capacitor) 200 μF (Electrolytic capacitor)

TABLE IV
PARAMETER VALUES OF THE CONVERTERS

Parameters	Value
V_{IN}	400 V
V_{O_ref}	5 V
V_A	8 V
$I_{O\_\max}$	25 A
$\Delta V_{O\_sw\_\max}$	±5% of V_{O_ref}
$\Delta V_{O\_Tr\_\max}$	1% of V_{O_ref}
ΔI_O	10 A
F_{sF}	50 kHz
F_{sA}, F_{sP}	250 kHz
f_{CF}	5 kHz (1/10th of F_{sF})
f_{CA}, f_{CP}	25 kHz (1/10th of F_{sA})

where $\Delta V_{A\_Tr\_\max} = 0.2V_A$. Table III shows the passive component results with a reference to the design margin.

B. Inductor Reduction

First, the inductance of L_F is designed. The inductance of L_F for a conventional forward converter is greater than that of the other cases because the output capacitance is limited for practical reasons, such as a start-up issue.

The start-up issue is when an over current problem can occur for charging the output capacitor if its capacitance is large. Thus, this inductance is greater than the optimum value given for the voltage ripple. On the other hand, L_F in the proposed method is not affected by this issue. Therefore, its inductance can be reduced. The minimum inductance of the proposed method with the given specification, L_F is determined as follows:

$$L_F = \frac{(1-D_F)V_O}{F_{sF}I_{LF\_pkpk}}. \quad (23)$$

In this paper, the inductance of L_F is designed for the peak value of i_{LF} to be less than 120% of $I_{O\_\max}$. In general, the core of an inductor is established using the following criterion [30]:

$$A_P \geq K_{AP}LI_{pk}^{\ 2}\,[cm^4], \quad (24)$$

where K_{AP} is a constant value [30], and the area product, A_P is a parameter which determines the core size. The minimum A_P- value of the output inductor L_F is reduced as shown below.

$$\Delta A_{P\_LF\_\min} = K_{AP}\left(L_{F(SF)}I_{LF\_pk\_SF}^{\ 2} - L_{F(AOF)}I_{LF\_pk\_AOF}^{\ 2}\right), \quad (25)$$

where:

$$I_{LF\_pk\_SF} = I_{O\_\max} + \frac{1}{2}I_{LF\_pkpk\_SF}, \quad (26)$$

$$I_{LF\_pk\_AOF} = I_{O\_\max} + \frac{1}{2}I_{LF\_pkpk\_AOF}. \quad (27)$$

An A_P comparison between the proposed method ($A_{P\_AOF\_\min}$) and the post-regulator method ($A_{P\_PR\_\min}$), for additional inductors, is given below.

$$A_{P\_AOF} = \frac{\left(\frac{1}{2}I_{LF\_pkpk\_AOF}\right)^2}{\left(I_{O\_\max} + \frac{1}{2}I_{LF\_pkpk\_PR}\right)^2}A_{P\_PR}. \quad (28)$$

Fig. 9 shows the A_P-values of the additional inductors, L_A and L_P, versus the switching frequency of the forward converter. The A_P-value of L_A is less than 2% that of L_F, even in the worst case, while that of the L_P is 10~30% that of the main converter. The A_P result does not satisfy the 'I_{LF_pkpk}<1.2$I_{O_\max}$' condition. The normalized total A_P-value of the proposed method is shown in Fig. 10. The proposed method shows an A_P–value which is reduced by half, even with the lower output inductance and lower switching frequency of the forward converter.

To verify the analysis of the proposed method, a hardware prototype of a 125-W forward converter with an AOF and a post-regulator is built and tested. First, the passive parameters are determined following the criteria in Section III. *A*. The results are compared with a conventional single-forward converter (SF) and a forward converter with a post-regulator (PR). Next, proper voltage controllers are designed based on the results in Section III. *B*. The target specifications are shown in Table IV.

C. Controller Design

Fig. 11 shows the transfer functions G_{vAdF} and G_{vOdA} of the hardware. As mentioned in Section III, G_{vOdA} shows a zero DC gain due to the +20 dB/decade slope of the low-frequency region. Thus, conventional voltage controllers with an integrator, such as a type-3 compensator, cannot achieve an infinite DC gain for a zero steady state error. Fortunately, this problem will be corrected after the v_A control loop is closed. Thus, only the high-frequency characteristic is an issue. After the design of H_{vO}, T_2 is designed with a proper H_{vA}. Because H_{vO} was previously designed, H_{vA} is designed using the total v_A voltage loop, T_{vA}. Two-pole-two-zero with one integrator controllers are utilized for H_{vO} and H_{vA}. These results are shown in Fig. 12.

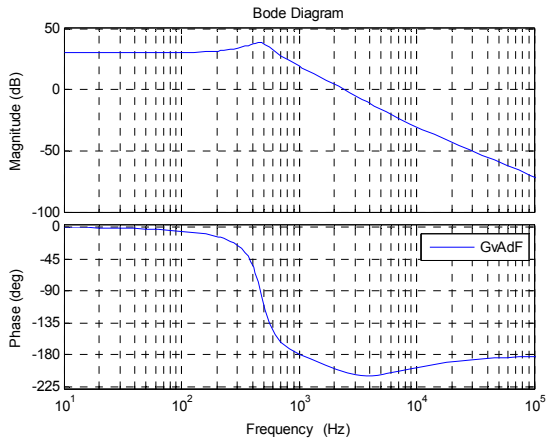

(a)

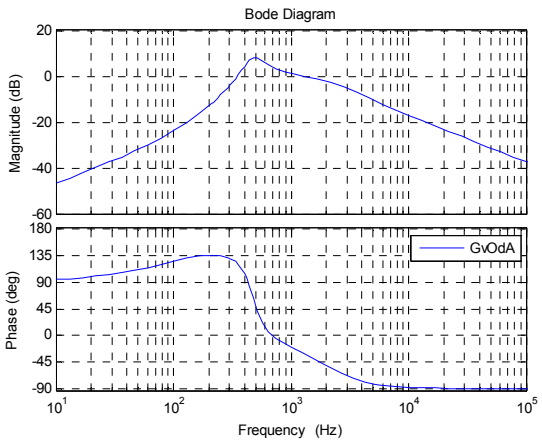

(b)

Fig. 11. Bode plots of transfer functions of the proposed system (opened-loop), (a) G_{vAdF}, (b) G_{vOdA}.

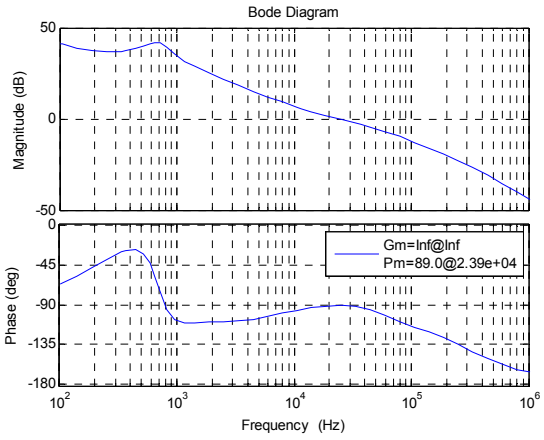

(a)

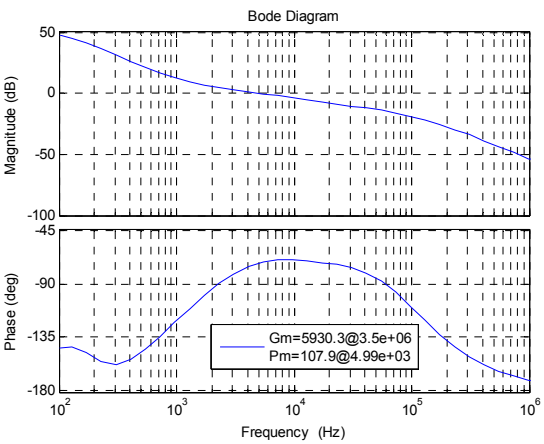

(b)

Fig. 12. Bode plot of closed-loop-gains, (a) T_{vO}, (b) T_{vA}.

V. EXPERIMENTAL RESULTS

To verify the proposed method, a forward converter hardware prototype is built and tested. The parameters follow the results shown in Section IV. A typical forward converter and a forward converter with a post-regulator are also built for comparison with the proposed method. The tests focus on three points: the voltage regulation, the volume, and the power efficiency. Fig. 13 shows the key waveforms under the steady state with the proposed method. The output voltage ripple satisfies the switching voltage ripple regulation range, 50 mV. In addition, Fig. 14 shows a 5 A step-up load transient response, which satisfies the voltage regulation, 250 mV. A comparison of the volumes between the proposed method and the conventional methods is briefly described in Fig. 15. The total volume of the inductors and capacitors of the proposed method is reduced by about 31.5% (20.9 cm^3) and by approximately 13.1% (8.7 cm^3) when compared to the conventional forward converter method and the post-regulator method, respectively. Fig. 16 shows the results of a power efficiency comparison. The efficiency of the proposed method is between those of the conventional forward converter method and the post regulator

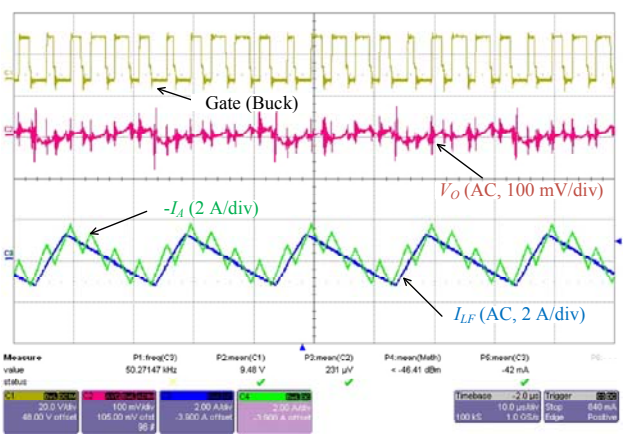

Fig. 13. Key waveforms in a steady state.

method. The proposed method shows only a 1% lower efficiency when compared to the conventional single forward converter case. The efficiency of the proposed method is 1~3% higher than that of the fast switching conventional single forward converter case and 2~8% higher than that of the post-regulator case, which are conventional approaches for passive component reduction. As a result, the proposed method achieves a passive component reduction without significantly losing efficiency.

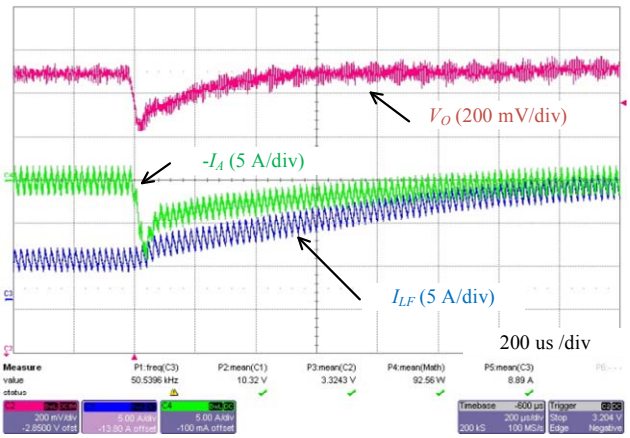

Fig. 14. Key waveforms during a step-up load transient.

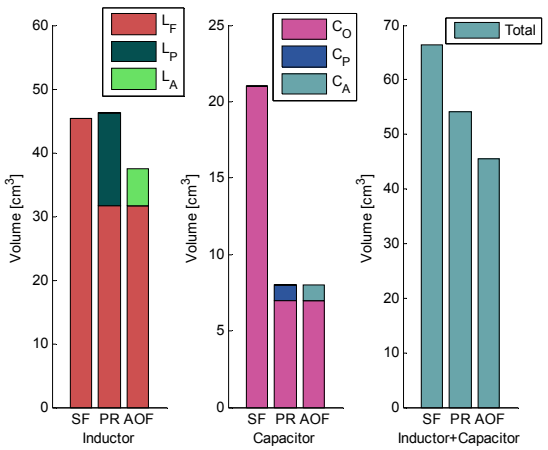

Fig. 15. Passive component volume comparison. (SF: a conventional single forward converter case, PR: a conventional post-regulator case, AOF: the proposed method case).

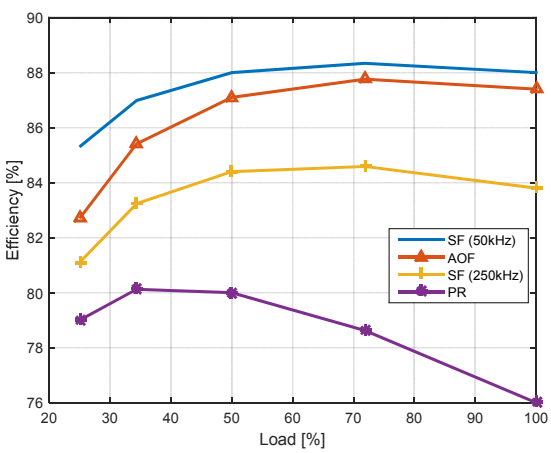

Fig. 16. Power efficiency comparion.

VI. Conclusion

In this paper, a novel POF reduction method is presented and analyzed. The proposed method reduces the POF while satisfying the output voltage regulations and demands for improved power efficiency. The proposed control strategy makes AOFs feasible for the voltage regulation of both the switching voltage ripple and voltage variations which arise during a load transient. A small signal analysis was done to ensure a stable and optimized system, and a design guideline was described. The volume of the POF is significantly reduced while the total efficiency is only slightly reduced. In addition, the results can be extended to other buck-type topologies such as buck converters and half/full-bridge converters, because operation algorithms and small signal models of these converters are practically the same. In addition, the proposed method can be extended to other PWM-based-converters by a similar procedure.

References

[1] Intel Corp., "Power supply – Design guide for desktop platform form factors," Rev. 1.31, Apr. 2013.

[2] Intel Corp., "Voltage regulator module (VRM) and enterprise voltage regulator-down (EVRD) 11.1," Sep. 2009.

[3] Ecos Consulting -80Plus- http://www.plugloadsolutions.com/80pluspowersupplies.asas, Aug. 26th 2015.

[4] D. C. Hamill and P. T. Krein, "A `zero' ripple technique applicable to any DC converter," in *Proc. PESC*, pp. 1165-1171, Vol. 2, 1999.

[5] J. Stahl, R. Junghaenel, M. Schmidt, and M. Albach, "Smoothing transformer as effective differential mode filter," in *Proc. APEMC*, pp. 277-280, 2012.

[6] M. J. Schutten, R. L. Steigerwald, and J. A. Sabaté, "Ripple current cancellation circuit," in *Proc. APEC*, pp. 464-470, Vol. 1, 2003.

[7] A. K. Guru, J. C. Balda, K. Carr, and Y. Q. Xiang, "Design of a switching-ripple filter for a shunt-connected active power filter," in *Proc. Industry Applications Conference*, pp. 1364-1368, Vol. 2, 1998.

[8] M. Zhu, D. J. Perreault, V. Caliskan, T. C. Neugebauer, S. Guttowski, and J. G. Kassakian, "Design and evaluation of feedforward active ripple filters," *IEEE Trans. Power Electron.*, Vol. 20, No. 2, pp. 276-284, Mar. 2005.

[9] M. S. Moon and B. H. Cho, "Novel active ripple filter for the solar array shunt switching unit," *Journal of Propulsion and Power*, Vol. 12, No. 1, pp. 78- 82, Jul./Fab. 1995.

[10] N. K. Poon, J. C. P. Liu, C. K. Tse, and M. H. Pong, "Techniques for input ripple current cancellation: classification and implementation," *IEEE Trans. Power Electron.*, Vol. 15, No. 6, pp. 1144-1152, Nov. 2000.

[11] J. Pforr, "Switch-mode current amplifier with high output current quality employing an active output filter," in *Proc. Power Electronics and Intelligent Motion Conference*, pp. 22–24, 1999.

[12] H. Ertl, J. W. Kolar, G. Morauf, and F. C. Zach, "Analysis of active ripple current compensators employing multi-cell switch-mode amplifier topologies," in *Proc. PCIM*, pp. 1-7, 2002.

[13] Z. Chen, M. Chen, Y. Luo, C. Wang, "Low frequency ripple current compensation with DC active filter for the single-phase aeronautic static inverter," in *Proc. ECCE*, pp. 1468-1475, Sep. 2011.

[14] D. Goder and W. R. Pelletier, "V^2 architecture provides ultra-fast transient response in switch mode power

supplies," in *Proc. High Frequency Power Conversion Conference*, pp. 19-23, 1996.
[15] W. Huang, "A new control for multi-phase buck converter with fast transient response," in *Proc. APEC*, pp. 273-279, Vol. 1, 2001.
[16] S. Qu, "Modeling and design considerations of V^2 controlled buck regulator," in *Proc. APEC*, pp. 507-513, Vol. 1, 2001.
[17] S. C. Tan, Y. M. Lai, C. K. Tse, and M. K. H. Cheung, "An adaptive sliding mode controller for buck converter in continuous conduction mode," in *Proc. APEC*, pp. 1395-1400, Vol. 3, 2004.
[18] D. Bieal, E. Fossas, F. Guinjoan, E. Alarcon, and A. Poveda "Application of sliding-mode control to the design of a buck-based sinusoidal generator," *IEEE Trans. Ind. Electron.*, Vol. 48, No. 3, pp. 563-571, Jun. 2002.
[19] S. Li, X. Zou, and X. Chen, "A nonlinear control buck converter with fast transient response," in *Proc. ISIC* pp. 45-48, 2009.
[20] A. Barrado, R. Vazquez, A. Lazaro, J. Pleite, J. Vazquez, and E. Olias, "Stability analysis of linear-non linear control (LnLc) applied to fast transient response DC-DC converter," in *Proc. PESC* pp. 1175-1180, Vol. 3, 2003.
[21] A. Babazadeh and D. Maksimovic, "Hybrid digital adaptive control for fast transient response in synchronous buck DC–DC converters," *IEEE Trans. Power Electron.*, Vol. 24, No. 11, pp. 2625-2638, Nov. 2009.
[22] N. K. Poon, J. C. P. Liu, and M. H. Pong, "A low cost DC-DC stepping inductance voltage regulator with fast transient loading response," in *Proc. APEC*, pp. 268-272, Vol.1, 2001.
[23] D. D. C. Lu, J. C. P. Liu, F. N. K. Poon, and B. M. H. Pong, "A single phase voltage regulator module (VRM) with stepping inductance for fast transient response," *IEEE Trans. Power Electron.*, Vol. 22, No. 2, pp. 417-424, Mar. 2007.
[24] Z. Shan, S. C. Tan, and C. K. Tse, "Transient mitigation of DC–DC converters for high output current slew rate applications," *IEEE Trans. Power Electron.*, Vol. 28, No. 5, pp. 2377-2388, May. 2013.
[25] Z. Shan, C. K. Tse, and S. C. Tan, "Classification of auxiliary circuit schemes for feeding fast load transients in switching power supplies," *IEEE Trans. Power Electron.*, Vol. 61, No. 3, pp. 930-942, Mar. 2014.
[26] Y. L. Lin and K. H. Liu, "A new synchronous-switch post regulator for multi-output forward converters," in *Proc. APEC*, pp. 693-696, 1990.
[27] B. C. Hyun and B. H. Cho, "The study of the asymmetrical half-bridge converter with magnetic coupled post regulator," in *Proc. KIPE*, pp. 121-123, Nov. 2007.
[28] X. Wang, F. Tian, and I. Batarseh, "High efficiency parallel post regulator for wide range input DC–DC converter," *IEEE Trans. Power Electron.*, Vol. 23, No. 2, pp. 852-858, Mar. 2008.
[29] K. Yao, Y. Ren, and F. C. Lee, "Critical bandwidth for the load transient response of voltage regulator modules," *IEEE Trans. Power Electron.*, Vol. 19, No. 6, pp. 1454-1461, Nov. 2004.
[30] C. W. T. McLyman, *Transformer and Inductor Design Handbook*, 3rd ed., CRC Press, pp. 8-20, 8-21, 2004.

Kyusik Choi received his B.S. and Ph.D. degrees in Electrical Engineering and Computer Science from Seoul National University, Seoul, Korea. His current research interests include multiple output converters, high-efficiency under light load conditions, and active power filters. He is a Student Member of the IEEE and the Korean Institute of Power Electronics (KIPE).

Bo-Hyung Cho received his B.S. and M.S. degrees from the California Institute of Technology, Pasadena, CA, USA; and his Ph.D. degree from Virginia Polytechnic Institute and State University (Virginia Tech), Blacksburg, VA, USA, all in Electrical Engineering. Prior to his research at Virginia Tech, he was a member of the Technical Staff with the Department of Power Conversion Electronics, TRW Defense and Space System Group, USA. From 1982 to 1995, he was a Professor in the Department of Electrical Engineering, Virginia Tech. In 1995, he joined the School of Electrical Engineering, Seoul National University, Seoul, Korea, where he is presently working as a Professor. His current research interests include power electronics, the modeling, analysis, and control of spacecraft power processing equipment, and distributed power systems. Dr. Cho is a member of Tau Beta Pi. He was a recipient of the 1989 Presidential Young Investigator Award from the National Science Foundation. He chaired the 2006 IEEE Power Electronics Specialists Conference.